

Improved measurement of the absolute branching fraction of $D^+ \rightarrow \bar{K}^0 \mu^+ \nu_\mu$

BESIII Collaboration

M. Ablikim¹, M. N. Achasov^{9,f}, X. C. Ai¹, O. Albayrak⁵, M. Albrecht⁴, D. J. Ambrose⁴⁴, A. Amoroso^{49a,49c}, F. F. An¹, Q. An^{46,b}, J. Z. Bai¹, R. Baldini Ferroli^{20a}, Y. Ban³¹, D. W. Bennett¹⁹, J. V. Bennett⁵, M. Bertani^{20a}, D. Bettoni^{21a}, J. M. Bianchi⁴³, F. Bianchi^{49a,49c}, E. Boger^{23,d}, I. Boyko²³, R. A. Briere⁵, H. Cai⁵¹, X. Cai^{1,b}, O. Cakir^{40a}, A. Calcaterra^{20a}, G. F. Cao¹, S. A. Cetin^{40b}, J. F. Chang^{1,b}, G. Chelkov^{23,d,e}, G. Chen¹, H. S. Chen¹, H. Y. Chen², J. C. Chen¹, M. L. Chen^{1,b}, S. Chen⁴¹, S. J. Chen²⁹, X. Chen^{1,b}, X. R. Chen²⁶, Y. B. Chen^{1,b}, H. P. Cheng¹⁷, X. K. Chu³¹, G. Cibinetto^{21a}, H. L. Dai^{1,b}, J. P. Dai³⁴, A. Dbeysi¹⁴, D. Dedovich²³, Z. Y. Deng¹, A. Denig²², I. Denysenko²³, M. Destefanis^{49a,49c}, F. De Mori^{49a,49c}, Y. Ding²⁷, C. Dong³⁰, J. Dong^{1,b}, L. Y. Dong¹, M. Y. Dong^{1,b}, Z. L. Dou²⁹, S. X. Du⁵³, P. F. Duan¹, J. Z. Fan³⁹, J. Fang^{1,b}, S. S. Fang¹, X. Fang^{46,b}, Y. Fang¹, R. Farinelli^{21a,21b}, L. Fava^{49b,49c}, O. Fedorov²³, F. Feldbauer²², G. Felici^{20a}, C. Q. Feng^{46,b}, E. Fioravanti^{21a}, M. Fritsch^{14,22}, C. D. Fu¹, Q. Gao¹, X. L. Gao^{46,b}, X. Y. Gao², Y. Gao³⁹, Z. Gao^{46,b}, I. Garzia^{21a}, K. Goetzen¹⁰, L. Gong³⁰, W. X. Gong^{1,b}, W. Gradl²², M. Greco^{49a,49c}, M. H. Gu^{1,b}, Y. T. Gu¹², Y. H. Guan¹, A. Q. Guo¹, L. B. Guo²⁸, R. P. Guo¹, Y. Guo¹, Y. P. Guo²², Z. Haddadi²⁵, A. Hafner²², S. Han⁵¹, X. Q. Hao¹⁵, F. A. Harris⁴², K. L. He¹, T. Held⁴, Y. K. Heng^{1,b}, Z. L. Hou¹, C. Hu²⁸, H. M. Hu¹, J. F. Hu^{49a,49c}, T. Hu^{1,b}, Y. Hu¹, G. S. Huang^{46,b}, J. S. Huang¹⁵, X. T. Huang³³, X. Z. Huang²⁹, Y. Huang²⁹, Z. L. Huang^{27,a}, T. Hussain⁴⁸, Q. Ji¹, Q. P. Ji³⁰, X. B. Ji¹, X. L. Ji^{1,b}, L. W. Jiang⁵¹, X. S. Jiang^{1,b}, X. Y. Jiang³⁰, J. B. Jiao³³, Z. Jiao¹⁷, D. P. Jin^{1,b}, S. Jin¹, T. Johansson⁵⁰, A. Julin⁴³, N. Kalantar-Nayestanaki²⁵, X. L. Kang¹, X. S. Kang³⁰, M. Kavatsyuk²⁵, B. C. Ke⁵, P. Kiese²², R. Kliemt¹⁴, B. Kloss²², O. B. Kolcu^{40b,i}, B. Kopf⁴, M. Kornicer⁴², A. Kupsc⁵⁰, W. Kühn²⁴, J. S. Lange²⁴, M. Lara¹⁹, P. Larin¹⁴, C. Leng^{49c}, C. Li⁵⁰, Cheng Li^{46,b}, D. M. Li⁵³, F. Li^{1,b}, F. Y. Li³¹, G. Li¹, H. B. Li¹, H. J. Li¹, J. C. Li¹, Jin Li³², K. Li³³, K. Li¹³, Lei Li³, P. R. Li⁴¹, Q. Y. Li³³, T. Li³³, W. D. Li¹, W. G. Li¹, X. L. Li³³, X. N. Li^{1,b}, X. Q. Li³⁰, Y. B. Li², Z. B. Li³⁸, H. Liang^{46,b}, Y. F. Liang³⁶, Y. T. Liang²⁴, G. R. Liao¹¹, D. X. Lin¹⁴, B. Liu³⁴, B. J. Liu¹, C. X. Liu¹, D. Liu^{46,b}, F. H. Liu³⁵, Fang Liu¹, Feng Liu⁶, H. B. Liu¹², H. H. Liu¹⁶, H. H. Liu¹, H. M. Liu¹, J. Liu¹, J. B. Liu^{46,b}, J. P. Liu⁵¹, J. Y. Liu¹, K. Liu³⁹, K. Y. Liu²⁷, L. D. Liu³¹, P. L. Liu^{1,b}, Q. Liu⁴¹, S. B. Liu^{46,b}, X. Liu²⁶, Y. B. Liu³⁰, Z. A. Liu^{1,b}, Zhiqing Liu²², H. Loehner²⁵, X. C. Lou^{1,b,h}, H. J. Lu¹⁷, J. G. Lu^{1,b}, Y. Lu¹, Y. P. Lu^{1,b}, C. L. Luo²⁸, M. X. Luo⁵², T. Luo⁴², X. L. Luo^{1,b}, X. R. Lyu⁴¹, F. C. Ma²⁷, H. L. Ma¹, L. L. Ma³³, M. M. Ma¹, Q. M. Ma¹, T. Ma¹, X. N. Ma³⁰, X. Y. Ma^{1,b}, Y. M. Ma³³, F. E. Maas¹⁴, M. Maggiora^{49a,49c}, Y. J. Mao³¹, Z. P. Mao¹, S. Marcello^{49a,49c}, J. G. Messchendorp²⁵, J. Min^{1,b}, T. J. Min¹, R. E. Mitchell¹⁹, X. H. Mo^{1,b}, Y. J. Mo⁶, C. Morales Morales¹⁴, N. Yu. Muchnoi^{9,f}, H. Muramatsu⁴³, Y. Nefedov²³, F. Nerling¹⁴, I. B. Nikolaev^{9,f}, Z. Ning^{1,b}, S. Nisar⁸, S. L. Niu^{1,b}, X. Y. Niu¹, S. L. Olsen³², Q. Ouyang^{1,b}, S. Pacetti^{20b}, Y. Pan^{46,b}, P. Patteri^{20a}, M. Pelizaeus⁴, H. P. Peng^{46,b}, K. Peters^{10,j}, J. Pettersson⁵⁰, J. L. Ping²⁸, R. G. Ping¹, R. Poling⁴³, V. Prasad¹, H. R. Qi², M. Qi²⁹, S. Qian^{1,b}, C. F. Qiao⁴¹, L. Q. Qin³³, N. Qin⁵¹, X. S. Qin¹, Z. H. Qin^{1,b}, J. F. Qiu¹, K. H. Rashid⁴⁸, C. F. Redmer²², M. Ripka²², G. Rong¹, Ch. Rosner¹⁴, X. D. Ruan¹², A. Sarantsev^{23,g}, M. Savrié^{21b}, K. Schoenning⁵⁰, S. Schumann²², W. Shan³¹, M. Shao^{46,b}, C. P. Shen², P. X. Shen³⁰, X. Y. Shen¹, H. Y. Sheng¹, M. Shi¹, W. M. Song¹, X. Y. Song¹, S. Sosio^{49a,49c}, S. Spataro^{49a,49c}, G. X. Sun¹, J. F. Sun¹⁵, S. S. Sun¹, X. H. Sun¹, Y. J. Sun^{46,b}, Y. Z. Sun¹, Z. J. Sun^{1,b}, Z. T. Sun¹⁹, C. J. Tang³⁶, X. Tang¹, I. Tapan^{40c}, E. H. Thorndike⁴⁴, M. Tiemens²⁵, M. Ullrich²⁴, I. Uman^{40d}, G. S. Varner⁴², B. Wang³⁰, B. L. Wang⁴¹, D. Wang³¹, D. Y. Wang³¹, K. Wang^{1,b}, L. L. Wang¹, L. S. Wang¹, M. Wang³³, P. Wang¹, P. L. Wang¹, W. Wang^{1,b}, W. P. Wang^{46,b}, X. F. Wang³⁹, Y. Wang³⁷, Y. D. Wang¹⁴, Y. F. Wang^{1,b}, Y. Q. Wang²², Z. Wang^{1,b}, Z. G. Wang^{1,b}, Z. H. Wang^{46,b}, Z. Y. Wang¹, Z. Y. Wang¹, T. Weber²², D. H. Wei¹¹, P. Weidenkaff²², S. P. Wen¹, U. Wiedner⁴, M. Wolke⁵⁰, L. H. Wu¹, L. J. Wu¹, Z. Wu^{1,b}, L. Xia^{46,b}, L. G. Xia³⁹, Y. Xia¹⁸, D. Xiao¹, H. Xiao⁴⁷, Z. J. Xiao²⁸, Y. G. Xie^{1,b}, Q. L. Xiu^{1,b}, G. F. Xu¹, J. J. Xu¹, L. Xu¹, Q. J. Xu¹³, Q. N. Xu⁴¹, X. P. Xu³⁷, L. Yan^{49a,49c}, W. B. Yan^{46,b}, W. C. Yan^{46,b}, Y. H. Yan¹⁸, H. J. Yang³⁴, H. X. Yang¹, L. Yang⁵¹, Y. X. Yang¹¹, M. Ye^{1,b}, M. H. Ye⁷, J. H. Yin¹, B. X. Yu^{1,b}, C. X. Yu³⁰, J. S. Yu²⁶, C. Z. Yuan¹, W. L. Yuan²⁹, Y. Yuan¹, A. Yuncu^{40b,c}, A. A. Zafar⁴⁸, A. Zallo^{20a}, Y. Zeng¹⁸, Z. Zeng^{46,b}, B. X. Zhang¹, B. Y. Zhang^{1,b}, C. Zhang²⁹, C. C. Zhang¹, D. H. Zhang¹, H. H. Zhang³⁸, H. Y. Zhang^{1,b}, J. Zhang¹,

J. J. Zhang¹, J. L. Zhang¹, J. Q. Zhang¹, J. W. Zhang^{1,b}, J. Y. Zhang¹, J. Z. Zhang¹, K. Zhang¹, L. Zhang¹, S. Q. Zhang³⁰, X. Y. Zhang³³, Y. Zhang¹, Y. H. Zhang^{1,b}, Y. N. Zhang⁴¹, Y. T. Zhang^{46,b}, Yu Zhang⁴¹, Z. H. Zhang⁶, Z. P. Zhang⁴⁶, Z. Y. Zhang⁵¹, G. Zhao¹, J. W. Zhao^{1,b}, J. Y. Zhao¹, J. Z. Zhao^{1,b}, Lei Zhao^{46,b}, Ling Zhao¹, M. G. Zhao³⁰, Q. Zhao¹, Q. W. Zhao¹, S. J. Zhao⁵³, T. C. Zhao¹, Y. B. Zhao^{1,b}, Z. G. Zhao^{46,b}, A. Zhemchugov^{23,d}, B. Zheng⁴⁷, J. P. Zheng^{1,b}, W. J. Zheng³³, Y. H. Zheng⁴¹, B. Zhong²⁸, L. Zhou^{1,b}, X. Zhou⁵¹, X. K. Zhou^{46,b}, X. R. Zhou^{46,b}, X. Y. Zhou¹, K. Zhu¹, K. J. Zhu^{1,b}, S. Zhu¹, S. H. Zhu⁴⁵, X. L. Zhu³⁹, Y. C. Zhu^{46,b}, Y. S. Zhu¹, Z. A. Zhu¹, J. Zhuang^{1,b}, L. Zotti^{49a,49c}, B. S. Zou¹, J. H. Zou¹

- ¹ Institute of High Energy Physics, Beijing 100049, People's Republic of China
² Beihang University, Beijing 100191, People's Republic of China
³ Beijing Institute of Petrochemical Technology, Beijing 102617, People's Republic of China
⁴ Bochum Ruhr-University, 44780 Bochum, Germany
⁵ Carnegie Mellon University, Pittsburgh, PA 15213, USA
⁶ Central China Normal University, Wuhan 430079, People's Republic of China
⁷ China Center of Advanced Science and Technology, Beijing 100190, People's Republic of China
⁸ COMSATS Institute of Information Technology, Lahore, Defence Road, Off Raiwind Road, 54000 Lahore, Pakistan
⁹ G.I. Budker Institute of Nuclear Physics SB RAS (BINP), Novosibirsk 630090, Russia
¹⁰ GSI Helmholtzcentre for Heavy Ion Research GmbH, 64291 Darmstadt, Germany
¹¹ Guangxi Normal University, Guilin 541004, People's Republic of China
¹² Guangxi University, Nanning 530004, People's Republic of China
¹³ Hangzhou Normal University, Hangzhou 310036, People's Republic of China
¹⁴ Helmholtz Institute Mainz, Johann-Joachim-Becher-Weg 45, 55099 Mainz, Germany
¹⁵ Henan Normal University, Xinxiang 453007, People's Republic of China
¹⁶ Henan University of Science and Technology, Luoyang 471003, People's Republic of China
¹⁷ Huangshan College, Huangshan 245000, People's Republic of China
¹⁸ Hunan University, Changsha 410082, People's Republic of China
¹⁹ Indiana University, Bloomington, IN 47405, USA
²⁰ (a) INFN Laboratori Nazionali di Frascati, 00044 Frascati, Italy;
 (b) INFN and University of Perugia, 06100 Perugia, Italy
²¹ (a) INFN Sezione di Ferrara, 44122 Ferrara, Italy;
 (b) University of Ferrara, 44122 Ferrara, Italy
²² Johannes Gutenberg University of Mainz, Johann-Joachim-Becher-Weg 45, 55099 Mainz, Germany
²³ Joint Institute for Nuclear Research, 141980 Dubna, Moscow region, Russia
²⁴ Justus-Liebig-Universität Giessen, II. Physikalisches Institut, Heinrich-Buff-Ring 16, 35392 Giessen, Germany
²⁵ KVI-CART, University of Groningen, 9747 AA Groningen, The Netherlands
²⁶ Lanzhou University, Lanzhou 730000, People's Republic of China
²⁷ Liaoning University, Shenyang 110036, People's Republic of China
²⁸ Nanjing Normal University, Nanjing 210023, People's Republic of China
²⁹ Nanjing University, Nanjing 210093, People's Republic of China
³⁰ Nankai University, Tianjin 300071, People's Republic of China
³¹ Peking University, Beijing 100871, People's Republic of China
³² Seoul National University, Seoul 151-747, Korea
³³ Shandong University, Jinan 250100, People's Republic of China
³⁴ Shanghai Jiao Tong University, Shanghai 200240, People's Republic of China
³⁵ Shanxi University, Taiyuan 030006, People's Republic of China
³⁶ Sichuan University, Chengdu 610064, People's Republic of China
³⁷ Soochow University, Suzhou 215006, People's Republic of China
³⁸ Sun Yat-Sen University, Guangzhou 510275, People's Republic of China
³⁹ Tsinghua University, Beijing 100084, People's Republic of China
⁴⁰ (a) Ankara University, 06100 Tandogan, Ankara, Turkey;
 (b) Istanbul Bilgi University, Eyup, 34060 Istanbul, Turkey;
 (c) Uludag University, 16059 Bursa, Turkey;
 (d) Near East University, Mersin 10, Nicosia, North Cyprus, Turkey
⁴¹ University of Chinese Academy of Sciences, Beijing 100049, People's Republic of China
⁴² University of Hawaii, Honolulu, HI 96822, USA
⁴³ University of Minnesota, Minneapolis, MN 55455, USA
⁴⁴ University of Rochester, Rochester, NY 14627, USA
⁴⁵ University of Science and Technology Liaoning, Anshan 114051, People's Republic of China
⁴⁶ University of Science and Technology of China, Hefei 230026, People's Republic of China
⁴⁷ University of South China, Hengyang 421001, People's Republic of China
⁴⁸ University of the Punjab, Lahore 54590, Pakistan
⁴⁹ (a) University of Turin, 10125 Turin, Italy;
 (b) University of Eastern Piedmont, 15121 Alessandria, Italy;
 (c) INFN, 10125 Turin, Italy
⁵⁰ Uppsala University, Box 516, 75120 Uppsala, Sweden

⁵¹ Wuhan University, Wuhan 430072, People's Republic of China

⁵² Zhejiang University, Hangzhou 310027, People's Republic of China

⁵³ Zhengzhou University, Zhengzhou 450001, People's Republic of China

Received: 2 May 2016 / Accepted: 12 June 2016 / Published online: 4 July 2016

© The Author(s) 2016. This article is published with open access at Springerlink.com

Abstract By analyzing 2.93 fb^{-1} of data collected at $\sqrt{s} = 3.773 \text{ GeV}$ with the BESIII detector, we measure the absolute branching fraction $\mathcal{B}(D^+ \rightarrow \bar{K}^0 \mu^+ \nu_\mu) = (8.72 \pm 0.07_{\text{stat.}} \pm 0.18_{\text{sys.}}) \%$, which is consistent with previous measurements within uncertainties but with significantly improved precision. Combining the Particle Data Group values of $\mathcal{B}(D^0 \rightarrow K^- \mu^+ \nu_\mu)$, $\mathcal{B}(D^+ \rightarrow \bar{K}^0 e^+ \nu_e)$, and the lifetimes of the D^0 and D^+ mesons with the value of $\mathcal{B}(D^+ \rightarrow \bar{K}^0 \mu^+ \nu_\mu)$ measured in this work, we determine the following ratios of partial widths: $\Gamma(D^0 \rightarrow K^- \mu^+ \nu_\mu) / \Gamma(D^+ \rightarrow \bar{K}^0 \mu^+ \nu_\mu) = 0.963 \pm 0.044$ and $\Gamma(D^+ \rightarrow \bar{K}^0 \mu^+ \nu_\mu) / \Gamma(D^+ \rightarrow \bar{K}^0 e^+ \nu_e) = 0.988 \pm 0.033$.

1 Introduction

Experimental studies of D semileptonic decays provide helpful information to understand D decay mechanisms. Their decay branching fractions (\mathcal{B}) can serve to test isospin conservation and leptonic universality in D semileptonic decays. Isospin conservation implies that the partial widths (Γ) of $D^0 \rightarrow K^- \mu^+ \nu_\mu$ and $D^+ \rightarrow \bar{K}^0 \mu^+ \nu_\mu$ should be equal. Furthermore, Ref. [1] predicts that $\Gamma(D \rightarrow \bar{K} \mu^+ \nu_\mu)$ is less than $\Gamma(D \rightarrow \bar{K} e^+ \nu_e)$ by about 3% due to different form factors and phase space. Using the branching fractions and the lifetimes of the D^0 and D^+ mesons (τ_{D^0} , τ_{D^+}), taken from the Particle Data Group (PDG) [2], we obtain $\Gamma(D^0 \rightarrow K^- \mu^+ \nu_\mu) / \Gamma(D^+ \rightarrow \bar{K}^0 \mu^+ \nu_\mu) = 0.91 \pm 0.07$ and $\Gamma(D^+ \rightarrow \bar{K}^0 \mu^+ \nu_\mu) / \Gamma(D^+ \rightarrow \bar{K}^0 e^+ \nu_e) = 1.04 \pm 0.07$, where the uncertainties are dominated by $\mathcal{B}(D^+ \rightarrow \bar{K}^0 \mu^+ \nu_\mu)$ [2]. Thus, an improved measurement of $\mathcal{B}(D^+ \rightarrow \bar{K}^0 \mu^+ \nu_\mu)$ will be helpful to understand D decay

mechanisms with better accuracy. In addition, the improved $\mathcal{B}(D^+ \rightarrow \bar{K}^0 \mu^+ \nu_\mu)$ can also be used to precisely determine the form factor $f_+^K(0)$ and the quark mixing matrix element $|V_{cs}|$ from D semileptonic decays [3].

Previous measurements of $\mathcal{B}(D^+ \rightarrow \bar{K}^0 \mu^+ \nu_\mu)$ come from MARKIII [4], FOCUS [5] and BESII [6]. In this paper, by analyzing 2.93 fb^{-1} of data [7, 8] collected at the center-of-mass energy of $\sqrt{s} = 3.773 \text{ GeV}$ by the BESIII detector [9], we determine the absolute branching fraction of $D^+ \rightarrow \bar{K}^0 \mu^+ \nu_\mu$. Throughout the paper, charge conjugation is implied.

2 BESIII detector and Monte Carlo

The BESIII detector is a cylindrical detector with a solid-angle coverage of 93% of 4π that operates at the BEPCII collider. It consists of several main components. A 43-layer main drift chamber (MDC) surrounding the beam pipe performs precise determinations of charged particle trajectories and provides a measurement of the specific ionization energy loss (dE/dx) that is used for charged particle identification (PID). An array of time-of-flight counters (TOF) is located radially outside the MDC and provides additional PID information. A CsI(Tl) electromagnetic calorimeter (EMC) surrounds the TOF and is used to measure the energies of photons and electrons. A solenoidal superconducting magnet located outside the EMC provides a 1 T magnetic field in the central tracking region of the detector. The iron flux return of the magnet is instrumented with about 1272 m^2 of resistive plate muon counters (MUC) arranged in nine layers in the barrel and eight layers in the endcaps that are used to identify muons with momentum greater than $0.5 \text{ GeV}/c$. More details about the BESIII detector are described in Ref. [9].

A GEANT4-based [10] Monte Carlo (MC) simulation software package, which includes the geometric description of the detector and its response, is used to determine the detection efficiency and to estimate the potential backgrounds. An inclusive MC sample, which includes the $D^0 \bar{D}^0$, $D^+ D^-$, and non- $D \bar{D}$ decays of $\psi(3770)$, the initial state radiation (ISR) production of $\psi(3686)$ and J/ψ , the $q\bar{q}$ ($q = u, d, s$) continuum process, the Bhabha scattering events, and the dimuon and di-tau events, is produced at $\sqrt{s} = 3.773 \text{ GeV}$. The $\psi(3770)$ decays are generated by the MC generator KKMC [11, 12], in which ISR effects [13, 14] and final state radi-

^a e-mail: huangzli@ihep.ac.cn

^b Also at State Key Laboratory of Particle Detection and Electronics, Beijing 100049, Hefei 230026, People's Republic of China

^c Also at Bogazici University, 34342 Istanbul, Turkey

^d Also at the Moscow Institute of Physics and Technology, Moscow 141700, Russia

^e Also at the Functional Electronics Laboratory, Tomsk State University, Tomsk 634050, Russia

^f Also at the Novosibirsk State University, Novosibirsk, 630090, Russia

^g Also at the NRC "Kurchatov Institute", PNPI, 188300, Gatchina, Russia

^h Also at University of Texas at Dallas, Richardson, TX 75083, USA

ⁱ Also at Istanbul Arel University, 34295 Istanbul, Turkey

^j Also at Goethe University Frankfurt, 60323 Frankfurt am Main, Germany

ation (FSR) effects [15] are simulated. The known decay modes of the charmonium states are generated using EvtGen [16, 17] with the branching fractions set to PDG values [18], and others are generated using LundCharm [19]. The $D^+ \rightarrow \bar{K}^0 \mu^+ \nu_\mu$ signal is simulated with the modified pole model [20].

3 Method

In e^+e^- collisions at $\sqrt{s} = 3.773$ GeV, the $\psi(3770)$ resonance decays predominately into a $D^0 \bar{D}^0$ or a $D^+ D^-$ pair. In an event where a D^- meson (called the single tag (ST) D^- meson) is fully reconstructed, the presence of a D^+ meson is guaranteed. In the systems recoiling against the ST D^- mesons, we can select the semileptonic decays of $D^+ \rightarrow \bar{K}^0 \mu^+ \nu_\mu$ (called the double tag (DT) events). For a special ST mode i , the ST and DT yields observed in data are given by

$$N_{ST}^i = 2N_{D^+D^-} \mathcal{B}_{ST}^i \epsilon_{ST}^i, \tag{1}$$

and

$$N_{DT}^i = 2N_{D^+D^-} \mathcal{B}_{ST}^i \mathcal{B}(D^+ \rightarrow \bar{K}^0 \mu^+ \nu_\mu) \epsilon_{ST, D^+ \rightarrow \bar{K}^0 \mu^+ \nu_\mu}^i, \tag{2}$$

where $N_{D^+D^-}$ is the number of $D^+ D^-$ pairs produced in data, \mathcal{B}_{ST}^i and $\mathcal{B}(D^+ \rightarrow \bar{K}^0 \mu^+ \nu_\mu)$ are the branching fractions for the ST mode i and the $D^+ \rightarrow \bar{K}^0 \mu^+ \nu_\mu$ decay, ϵ_{ST}^i is the efficiency of reconstructing the ST mode i (called the ST efficiency), and $\epsilon_{ST, D^+ \rightarrow \bar{K}^0 \mu^+ \nu_\mu}^i$ is the efficiency of simultaneously finding the ST mode i and the $D^+ \rightarrow \bar{K}^0 \mu^+ \nu_\mu$ decay (called the DT efficiency). Based on these two equations, the absolute branching fraction for $D^+ \rightarrow \bar{K}^0 \mu^+ \nu_\mu$ can be determined by

$$\mathcal{B}(D^+ \rightarrow \bar{K}^0 \mu^+ \nu_\mu) = \frac{N_{DT}^{tot}}{N_{ST}^{tot} \bar{\epsilon}_{D^+ \rightarrow \bar{K}^0 \mu^+ \nu_\mu}}, \tag{3}$$

where $\bar{\epsilon}_{D^+ \rightarrow \bar{K}^0 \mu^+ \nu_\mu} = \sum_i (N_{ST}^i \epsilon_{ST, D^+ \rightarrow \bar{K}^0 \mu^+ \nu_\mu}^i / \epsilon_{ST}^i) / N_{ST}^{tot}$ is the averaged efficiency of reconstructing the $D^+ \rightarrow \bar{K}^0 \mu^+ \nu_\mu$ decay by the ST yields in data.

4 ST D^- mesons

The ST D^- mesons are reconstructed using six hadronic decay modes: $K^+ \pi^- \pi^-$, $K_S^0 \pi^-$, $K^+ \pi^- \pi^- \pi^0$, $K_S^0 \pi^- \pi^0$, $K_S^0 \pi^+ \pi^- \pi^-$ and $K^+ K^- \pi^-$. The decays of K_S^0 and π^0

mesons are identified in $K_S^0 \rightarrow \pi^+ \pi^-$ and $\pi^0 \rightarrow \gamma \gamma$, respectively.

All charged tracks used in this analysis are required to be within a polar-angle (θ) range of $|\cos \theta| < 0.93$. Except for those from K_S^0 decays, all tracks are required to originate from an interaction region defined by $V_{xy} < 1.0$ cm and $|V_z| < 10.0$ cm, where V_{xy} and $|V_z|$ refer to the distances of closest approach of the reconstructed track to the Interaction Point (IP) in the xy plane and the z direction (along the beam), respectively.

The charged kaons and pions are identified by the dE/dx and TOF information. The combined Confidence Levels for pion and kaon hypotheses (CL_π and CL_K) are calculated, respectively. A charged track is identified as a kaon (pion) if the confidence levels satisfy $CL_K > CL_\pi$ ($CL_\pi > CL_K$).

The charged tracks from K_S^0 decays are required to satisfy $|V_z| < 20.0$ cm. The two oppositely charged tracks are assigned as $\pi^+ \pi^-$ without PID. The $\pi^+ \pi^-$ pair is constrained to originate from a common vertex and is required to have an invariant mass within $|M_{\pi^+ \pi^-} - M_{K_S^0}| < 12$ MeV/ c^2 , where $M_{K_S^0}$ is the K_S^0 nominal mass [2]. The K_S^0 candidate is required to have a decay length larger than 2 standard deviations of the vertex resolution away from the IP.

Photon candidates are selected using the information from the EMC. It is required that the shower time be within 700 ns of the event start time, the shower energy be greater than 25 (50) MeV if the crystal with the maximum deposited energy in that cluster is in the barrel (endcap) region [9], and the opening angle between the candidate shower and any charged tracks be greater than 10° . To reconstruct π^0 , the invariant mass of the accepted $\gamma \gamma$ pair is required to be within (0.115, 0.150) GeV/ c^2 . To improve resolution, a kinematic fit is performed to constrain the $\gamma \gamma$ invariant mass to the π^0 nominal mass [2].

To identify the ST D^- mesons, we define two variables, the energy difference $\Delta E = E_{mKn\pi} - E_{beam}$ and the beam energy constrained mass $M_{BC} = \sqrt{E_{beam}^2 - |\vec{p}_{mKn\pi}|^2}$ of the $mKn\pi$ ($m = 1, 2; n = 1, 2, 3$) final states, where E_{beam} is the beam energy, $\vec{p}_{mKn\pi}$ and $E_{mKn\pi}$ are the measured momentum and energy of the $mKn\pi$ final state in the e^+e^- center-of-mass frame. For each ST mode, if there is more than one combination surviving, only the one with the minimum $|\Delta E|$ is kept. To suppress combinatorial backgrounds, ΔE is required to be within $(-25, +25)$ MeV for the $K^+ \pi^- \pi^-$, $K_S^0 \pi^-$, $K_S^0 \pi^+ \pi^- \pi^-$ and $K^+ K^- \pi^-$ final states, and be within $(-55, +40)$ MeV for the $K^+ \pi^- \pi^- \pi^0$ and $K_S^0 \pi^- \pi^0$ final states.

To obtain the ST yield, we apply a fit to the M_{BC} distributions of the accepted $mKn\pi$ final states for data. In the fits, the D^- signal is modeled by a MC-determined shape of the M_{BC} distribution convoluted with a double Gaussian func-

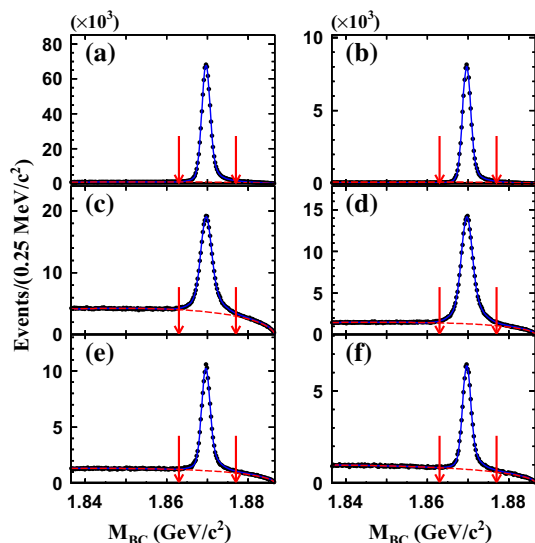


Fig. 1 Fits to the M_{BC} distributions of **a** $K^+\pi^-\pi^-\pi^-$, **b** $K_S^0\pi^-\pi^-$, **c** $K^+\pi^-\pi^-\pi^0$, **d** $K_S^0\pi^+\pi^-\pi^0$, **e** $K_S^0\pi^+\pi^-\pi^-\pi^0$ and **(f)** $K^+K^-\pi^-\pi^-$ combinations. The dots with error bars are data, the blue solid curves are the fit results, the red dashed curves are the fitted backgrounds and the pair of red arrows in each sub-figure denote the ST D^- signal region

tion and the combinatorial background shape is described by the ARGUS function [21]. The fit results are shown in Fig. 1. The candidates with M_{BC} in the range (1.863, 1.877) GeV/c^2 (signal region) are kept for further analysis. The ST yields and the ST efficiencies estimated from the inclusive MC sample are summarized in Table 1. The total ST yield is $N_{ST}^{\text{tot}} = 1522474 \pm 2215$.

5 DT events

From the surviving charged tracks and photons in the systems against the ST D^- mesons, the $D^+ \rightarrow \bar{K}^0\mu^+\nu_\mu$ candidates are selected with the following, optimized criteria. The \bar{K}^0 is reconstructed using the decays $\bar{K}^0 \rightarrow \pi^+\pi^-$ and $\bar{K}^0 \rightarrow \pi^0\pi^0$. To select $\bar{K}^0(\pi^0\pi^0)$, the $\pi^0\pi^0$ invariant mass is required to be within (0.45, 0.51) GeV/c^2 . If more than one combination survives, the one with the minimum $\chi_1^2(\pi^0 \rightarrow \gamma\gamma) + \chi_2^2(\pi^0 \rightarrow \gamma\gamma)$ is kept, where χ_1^2 and χ_2^2 are the chi-squares of the mass-constrained fits on $\pi^0 \rightarrow \gamma\gamma$. The good charged tracks, photons, π^0 , and $\bar{K}^0(\pi^+\pi^-)$ candidates are selected with the same criteria as those used in the ST selection.

We require that there be only one good additional charged track with charge opposite to that of the ST D^- meson. For muon identification, we combine the dE/dx , TOF and EMC information to calculate the Confidence Levels for electron, pion, kaon and muon hypotheses ($CL_e, CL_\pi, CL_K, CL_\mu$), respectively. The charged track is assigned as a muon candidate if the confidence levels satisfy $CL_\mu > CL_K$,

$CL_\mu > CL_e$ and $CL_\mu > 0.001$. To decrease the rate of mis-identifying pions as muons, we require that the energies deposited in the EMC by muons be within (0.1, 0.3) GeV.

Since the neutrino is undetectable, we define a kinematic quantity

$$U_{\text{miss}} \equiv E_{\text{miss}} - |\vec{p}_{\text{miss}}|,$$

where E_{miss} and $|\vec{p}_{\text{miss}}|$ are the energy and momentum of the missing particle in the DT event, respectively. E_{miss} is calculated by

$$E_{\text{miss}} = E_{\text{beam}} - E_{\bar{K}^0} - E_{\mu^+},$$

where $E_{\bar{K}^0}$ and E_{μ^+} are the measured energies of \bar{K}^0 and μ^+ , respectively. \vec{p}_{miss} is defined as

$$\vec{p}_{\text{miss}} = |\vec{p}_{D^+} - \vec{p}_{\bar{K}^0} - \vec{p}_{\mu^+}|,$$

where $\vec{p}_{\bar{K}^0}$ and \vec{p}_{μ^+} are the measured momenta of \bar{K}^0 and μ^+ , \vec{p}_{D^+} is the constrained momentum of D^+ meson

$$\vec{p}_{D^+} = (-\hat{p}_{D_{ST}^-})\sqrt{E_{\text{beam}}^2 - m_{D^+}^2},$$

where $\hat{p}_{D_{ST}^-}$ is the momentum direction of the ST D^- meson and m_{D^+} is the D^+ nominal mass [2].

Figures 2 and 3 show the distributions of the $\bar{K}^0\mu^+$ invariant masses ($M_{\bar{K}^0\mu^+}$) and the maximum energies ($E_{\text{max}}^{\text{extra } \gamma}$) of any of the extra photons which have not been used in the DT event selection from data and the inclusive MC sample, respectively, in which the backgrounds are dominated by $D^+ \rightarrow \bar{K}^0\pi^+(\pi^0)$. To suppress these backgrounds, we require that the $D^+ \rightarrow \bar{K}^0\mu^+\nu_\mu$ candidates have $M_{\bar{K}^0\mu^+} < 1.6 \text{ GeV}/c^2$ and $E_{\text{max}}^{\text{extra } \gamma} < 0.15 \text{ GeV}$.

The DT efficiency is determined by analyzing signal MC events. Dividing ϵ_{DT} by ϵ_{ST} , we obtain the efficiency of detecting $D^+ \rightarrow \bar{K}^0\mu^+\nu_\mu$ ($\epsilon_{D^+ \rightarrow \bar{K}^0\mu^+\nu_\mu}^{+-}$) for each ST mode. They are summarized in Table 1. The averaged efficiencies of detecting $D^+ \rightarrow \bar{K}^0\mu^+\nu_\mu$ are determined to be

$$\bar{\epsilon}_{D^+ \rightarrow \bar{K}^0\mu^+\nu_\mu}^{+-} = \frac{\sum_i (N_{ST}^i \epsilon_{D^+ \rightarrow \bar{K}^0\mu^+\nu_\mu}^{i,+-})}{N_{ST}^{\text{tot}}} = (35.97 \pm 0.11) \%$$

and

$$\bar{\epsilon}_{D^+ \rightarrow \bar{K}^0\mu^+\nu_\mu}^{00} = \frac{\sum_i (N_{ST}^i \epsilon_{D^+ \rightarrow \bar{K}^0\mu^+\nu_\mu}^{i,00})}{N_{ST}^{\text{tot}}} = (21.10 \pm 0.10) \%,$$

where the i denotes the sum over the six ST modes and $+-$ and 00 denote the $D^+ \rightarrow \bar{K}^0\mu^+\nu_\mu$ signals, which are reconstructed via $\bar{K}^0 \rightarrow \pi^+\pi^-$ and $\bar{K}^0 \rightarrow \pi^0\pi^0$, respectively.

To determine the signal yield, we perform simultaneous fits to the two U_{miss} distributions of the DT candidates, in which $D^+ \rightarrow \bar{K}^0\mu^+\nu_\mu$ is reconstructed via $\bar{K}^0 \rightarrow \pi^+\pi^-$ and $\bar{K}^0 \rightarrow \pi^0\pi^0$. In the fits, we constrain the numbers of the efficiency and branching fraction corrected DT events and $D^+ \rightarrow \bar{K}^0\pi^+\pi^0$ peaking backgrounds, respectively,

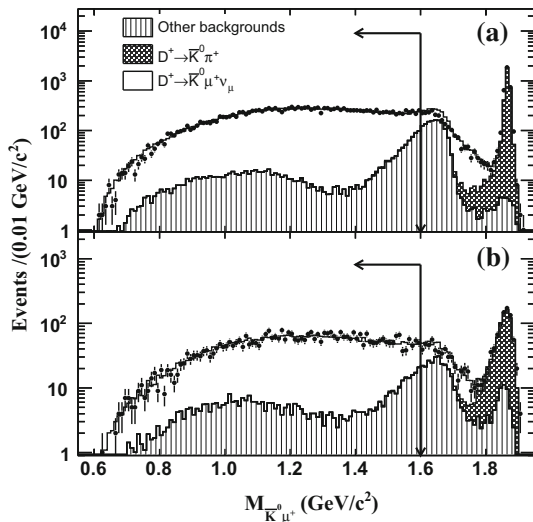


Fig. 2 The $M_{\bar{K}^0\mu^+}$ distributions of the **a** $D^+ \rightarrow \bar{K}^0(\pi^+\pi^-)\mu^+\nu_\mu$ and **b** $D^+ \rightarrow \bar{K}^0(\pi^0\pi^0)\mu^+\nu_\mu$ candidates of data (points with error bars) and the inclusive MC sample (histograms). The perpendicular black arrow shows the requirement $M_{\bar{K}^0\mu^+} < 1.6 \text{ GeV}/c^2$. Other backgrounds are dominated by $D^+ \rightarrow \bar{K}^0\pi^+\pi^0$. For this figure, U_{miss} is required to be within $(-0.06, +0.06) \text{ GeV}$

under the assumption that K_S^0 contributes to half of the neutral kaon decays. We use MC-determined shapes convoluted with Gaussian functions to describe the $D^+ \rightarrow \bar{K}^0\mu^+\nu_\mu$ signal and the $D^+ \rightarrow \bar{K}^0\pi^+\pi^0$ peaking background, and MC-based shape is also employed to represent the rest of the background and their overall normalizations are free parameters in the fits. The fit results are shown in Fig. 4. From the constrained fits, we determine the efficiency and branching fraction corrected DT production yield in data to be

$$N_{\text{DT}}^{\text{prd}} = 132712 \pm 1041,$$

corresponding to the observed DT yields $N_{\text{DT}}^{+-,\text{obs}} = 16516 \pm 130$ and $N_{\text{DT}}^{00,\text{obs}} = 4198 \pm 33$ for the $+-$ and 00 modes, respectively.

Table 1 Summary of the ST yields (N_{ST}^i), the ST and DT efficiencies (ϵ_{ST}^i and ϵ_{DT}^i), and the efficiencies of detecting $D^+ \rightarrow \bar{K}^0\mu^+\nu_\mu$ ($\epsilon_{D^+ \rightarrow \bar{K}^0\mu^+\nu_\mu}^i$). The efficiencies (in percent) do not include $\mathcal{B}(\pi^0 \rightarrow \gamma\gamma)$ and $\mathcal{B}(\bar{K}^0 \rightarrow \pi\pi)$. $+-$ and 00 denote the $D^+ \rightarrow \bar{K}^0\mu^+\nu_\mu$ signals, which are reconstructed via $\bar{K}^0 \rightarrow \pi^+\pi^-$ and $\bar{K}^0 \rightarrow \pi^0\pi^0$,

Tag mode	N_{ST}^i	ϵ_{ST}^i	$\epsilon_{\text{DT}}^{i,+}$	$\epsilon_{D^+ \rightarrow \bar{K}^0\mu^+\nu_\mu}^{i,+}$	$\epsilon_{\text{DT}}^{i,00}$	$\epsilon_{D^+ \rightarrow \bar{K}^0\mu^+\nu_\mu}^{i,00}$
$D^- \rightarrow K^+\pi^-\pi^-$	782669 ± 990	50.61 ± 0.06	17.96 ± 0.05	35.49 ± 0.11	10.75 ± 0.06	21.23 ± 0.13
$D^- \rightarrow K_S^0\pi^-$	91345 ± 320	50.41 ± 0.17	18.66 ± 0.16	37.00 ± 0.34	11.73 ± 0.20	23.26 ± 0.40
$D^- \rightarrow K^+\pi^-\pi^-\pi^0$	251008 ± 1135	26.74 ± 0.09	9.50 ± 0.05	35.52 ± 0.23	5.17 ± 0.06	19.34 ± 0.22
$D^- \rightarrow K_S^0\pi^-\pi^0$	215364 ± 1238	27.29 ± 0.07	10.71 ± 0.06	39.23 ± 0.24	6.11 ± 0.07	22.35 ± 0.26
$D^- \rightarrow K_S^0\pi^+\pi^-\pi^-$	113054 ± 889	28.31 ± 0.12	9.98 ± 0.08	35.26 ± 0.32	5.97 ± 0.09	21.08 ± 0.34
$D^- \rightarrow K^+K^-\pi^-$	69034 ± 460	40.83 ± 0.24	13.34 ± 0.14	32.69 ± 0.40	7.88 ± 0.17	19.31 ± 0.43

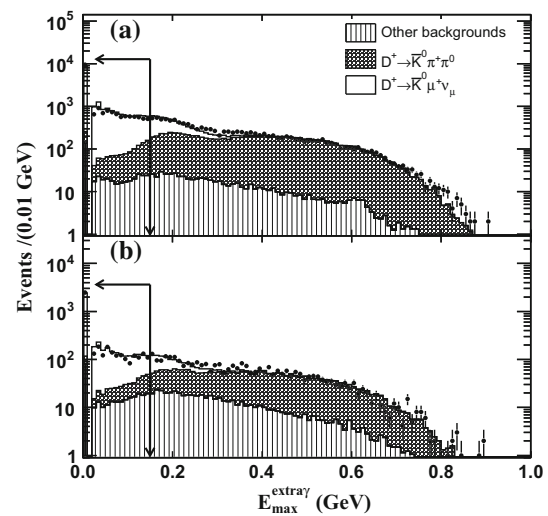


Fig. 3 The $E_{\text{max}}^{\text{extra } \gamma}$ distributions of the **a** $D^+ \rightarrow \bar{K}^0(\pi^+\pi^-)\mu^+\nu_\mu$ and **b** $D^+ \rightarrow \bar{K}^0(\pi^0\pi^0)\mu^+\nu_\mu$ candidates of data (points with error bars) and the inclusive MC sample (histograms). The perpendicular black arrow shows the requirement $E_{\text{max}}^{\text{extra } \gamma} < 0.15 \text{ GeV}$. For this figure, U_{miss} is required to be within $(-0.06, +0.06) \text{ GeV}$

We compare the $\cos\theta$ and momentum distributions of \bar{K}^0 and μ^+ as well as the $\pi\pi$ invariant mass distributions from the $D^+ \rightarrow \bar{K}^0(\pi^+\pi^-)\mu^+\nu_\mu$ and $D^+ \rightarrow \bar{K}^0(\pi^0\pi^0)\mu^+\nu_\mu$ candidates between data and MC, as shown in Figs. 5, 6 and 7, respectively. Here, U_{miss} is required to be within $(-0.06, +0.06) \text{ GeV}$, which includes about 98% of $D^+ \rightarrow \bar{K}^0(\pi^+\pi^-)\mu^+\nu_\mu$ and 86% of $D^+ \rightarrow \bar{K}^0(\pi^0\pi^0)\mu^+\nu_\mu$ signals. In these figures, we can see good agreement between data and MC.

6 Systematic uncertainty

The common systematic uncertainty in $\mathcal{B}(D^+ \rightarrow \bar{K}^0\mu^+\nu_\mu)$ measured with $\bar{K}^0 \rightarrow \pi^+\pi^-$ and $\bar{K}^0 \rightarrow \pi^0\pi^0$ arises from the uncertainties in the fits to the M_{BC} distributions,

respectively. The DT efficiencies have been corrected according to the differences of the efficiencies of the μ^+ tracking, the μ^+ PID, the π^0 reconstruction of the signal side and the $E_{\text{max}}^{\text{extra } \gamma}$ (see text) requirement between data and MC. The i represents the i th ST mode. The uncertainties are statistical only

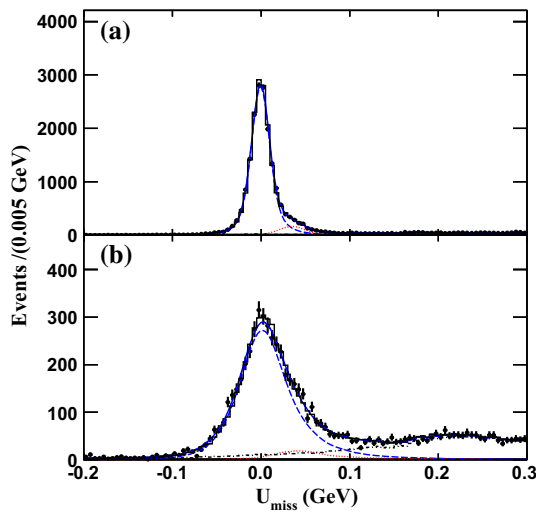


Fig. 4 Fits to the U_{miss} distributions of the **a** $D^+ \rightarrow \bar{K}^0(\pi^+\pi^-)\mu^+\nu_\mu$ and **b** $D^+ \rightarrow \bar{K}^0(\pi^0\pi^0)\mu^+\nu_\mu$ candidates, where the histograms are the inclusive MC sample, the dots with error bars are data, the blue solid curves are the fit results, the blue dashed curves are the $D^+ \rightarrow \bar{K}^0\mu^+\nu_\mu$ signals, the red dotted curves are the $D^+ \rightarrow \bar{K}^0\pi^+\pi^0$ peaking backgrounds and the black dot-dashed curves are from other backgrounds

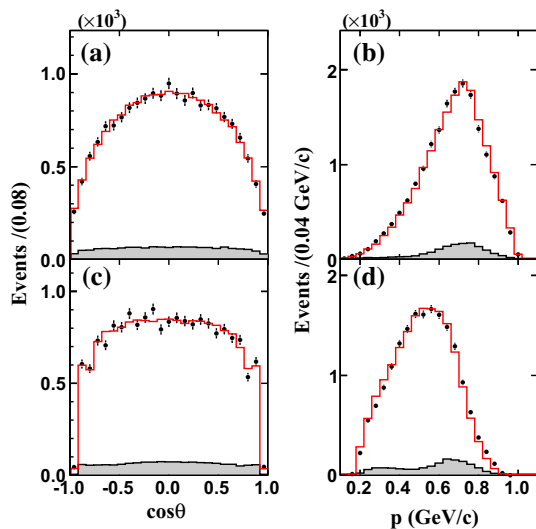


Fig. 5 Comparisons of the $\cos\theta$ and momentum distributions of **a, b** \bar{K}^0 and **c, d** μ^+ from the $D^+ \rightarrow \bar{K}^0(\pi^+\pi^-)\mu^+\nu_\mu$ candidates, where the dots with error bars are data, the red histograms are the inclusive MC sample, and the hatched histograms are the MC simulated backgrounds

the ΔE and M_{BC} requirements, the μ^+ tracking, the μ^+ PID, the $E_{\text{max}}^{\text{extra } \gamma}$ requirement, the $M_{\bar{K}^0\mu^+}$ requirement and the U_{miss} fit. The uncertainty in the fits to the M_{BC} distributions is estimated to be 0.5% by examining the relative change of the yields of data and MC via varying the fit range, the combinatorial background shape or the endpoint of the ARGUS function. To estimate the uncertainties in the ΔE and M_{BC} requirements, we examine the branching fractions by enlarging the ΔE windows by 5 or 10 MeV and varying

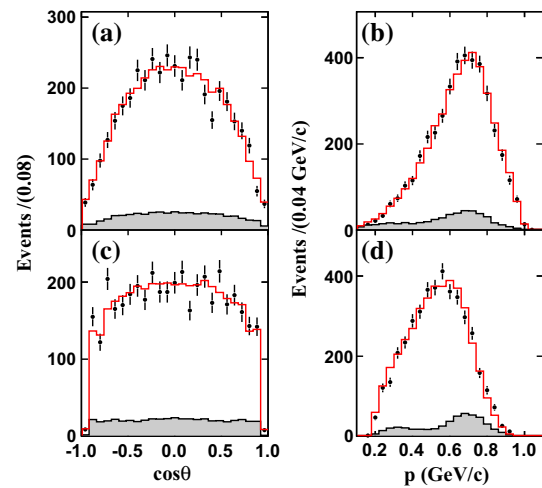


Fig. 6 Comparisons of the $\cos\theta$ and momentum distributions of **a, b** \bar{K}^0 and **c, d** μ^+ from the $D^+ \rightarrow \bar{K}^0(\pi^0\pi^0)\mu^+\nu_\mu$ candidates, where the dots with error bars are data, the red histograms are the inclusive MC sample, and the hatched histograms are the MC simulated backgrounds

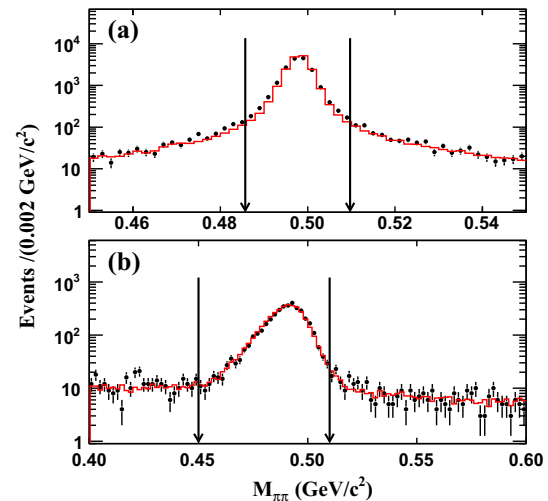


Fig. 7 Comparisons of the **a** $\pi^+\pi^-$ and **b** $\pi^0\pi^0$ distributions of the $D^+ \rightarrow \bar{K}^0\mu^+\nu_\mu$ candidates, where the dots with error bars are data, the red histograms are the inclusive MC sample and the arrow pairs denote the K^0 mass windows

the M_{BC} windows by ± 1 MeV/ c^2 , respectively. The maximum changes of the branching fractions, which are 0.3 and 0.3% for ΔE and M_{BC} requirements, are assigned as the uncertainties, respectively. The uncertainties in the tracking and PID for μ^+ are estimated by analyzing $e^+e^- \rightarrow \gamma\mu^+\mu^-$ events. The differences of the two-dimensional (momentum and $\cos\theta$) weighted tracking efficiencies of data and MC are determined to be $(+0.2 \pm 0.5)\%$ and $(-1.5 \pm 0.5)\%$, respectively. We assign 0.5 and 0.5% as the systematic uncertainties in the tracking and PID for μ^+ after correcting for these differences, respectively. Due to different topologies, there may be difference between the weighted efficiencies for the muons

in $D^+ \rightarrow \bar{K}^0 \mu^+ \nu_\mu$ and $e^+ e^- \rightarrow \gamma \mu^+ \mu^-$. This difference, which is estimated to be 0.5% by analyzing the two kinds of signal MC events, is considered as a systematic uncertainty. By examining the doubly tagged hadronic $D\bar{D}$ decays, we find that the difference of the acceptance efficiencies with $E_{\max}^{\text{extra } \gamma} < 0.15$ GeV of data and MC is $(+3.6 \pm 0.1)\%$. So, we assign 0.1% as the uncertainty in the $E_{\max}^{\text{extra } \gamma}$ requirement after correcting the MC efficiency to data. The uncertainty in the $M_{\bar{K}^0 \mu^+}$ requirement is estimated to be 0.8% by comparing the branching fractions measured with alternative requirements of $M_{\bar{K}^0 \mu^+} < 1.55$ and 1.65 GeV/ c^2 with the nominal value. The uncertainty in the U_{miss} fit is estimated to be 0.8% by comparing the branching fractions measured using different signal shape, background shape and fit range with the nominal value. Here, to examine the uncertainty in the background shape, we vary the relative strengths of each of the components in the inclusive MC sample and shift the estimated numbers of other peaking backgrounds by 1σ . In our previous work, the uncertainty in the signal MC generator is estimated to be 0.1%, which is obtained by comparing the DT efficiencies before and after re-weighting the $q^2 = (p_D - p_K)^2$ distribution of the signal MC events of $D^0 \rightarrow K^- e^+ \nu_e$ to data [23], where the p_D and p_K are the momenta of D and K mesons. Adding these in quadrature, we obtain the total common systematic uncertainty $\delta_{\text{sys}}^{\text{com}}$ to be 1.6%.

For the measurement with $\bar{K}^0 \rightarrow \pi^+ \pi^-$, the independent systematic uncertainty arises from the uncertainties in the $\bar{K}^0 \rightarrow \pi^+ \pi^-$ reconstruction, the MC statistics (0.4%), and $\mathcal{B}(\bar{K}^0 \rightarrow \pi^+ \pi^-)$ (0.1%) [2]. The uncertainty in the $\bar{K}^0 \rightarrow \pi^+ \pi^-$ reconstruction is estimated to be 1.5% by studying $J/\psi \rightarrow K^{*\mp} K^\pm$ and $J/\psi \rightarrow \phi \bar{K}^0 K^\pm \pi^\mp + c.c.$ events [22]. Adding these uncertainties in quadrature, we obtain the total independent systematic uncertainty ($\delta_{\text{sys}}^{\text{ind}}$) for $\bar{K}^0 \rightarrow \pi^+ \pi^-$ mode to be 1.6%.

For the measurement with $\bar{K}^0 \rightarrow \pi^0 \pi^0$, the independent systematic uncertainty arises from the uncertainties in the π^0 selection, the \bar{K}^0 mass window, the MC statistics (0.5%), $\mathcal{B}(\bar{K}^0 \rightarrow \pi^0 \pi^0)$ (0.2%) [2] and the $\chi_1^2 + \chi_2^2$ selection method. The π^0 reconstruction efficiency is verified by analyzing the hadronic decays $D^0 \rightarrow K^- \pi^+$ and $K^- \pi^+ \pi^+ \pi^-$ versus $\bar{D}^0 \rightarrow K^- \pi^+ \pi^0$ and $K_S^0(\pi^+ \pi^-) \pi^0$. The difference of the π^0 reconstruction efficiencies of data and MC is found to be $(-1.1 \pm 1.0)\%$ per π^0 . After correcting the detection efficiency of the signal side for this difference, the systematic uncertainty in π^0 reconstruction is taken as 1.0% per π^0 . Here, the photons from the $\bar{K}^0 \rightarrow K_S^0(\pi^0 \pi^0)$ decays are reconstructed under an assumption that the K_S^0 meson decayed at the IP. We investigate the DT efficiencies of two kinds of signal MC events, in which the lifetimes of K_S^0 meson from the signal side are set at the nominal value and 0, respectively. Their difference is less than 0.2%, which is considered as the systematic uncertainty of

the $K_S^0(\pi^0 \pi^0)$ reconstruction. To avoid the effect of the $D^+ \rightarrow \bar{K}^0 \pi^+ \pi^0$ peaking backgrounds, the uncertainty in the $\bar{K}^0(\pi^0 \pi^0)$ mass window is estimated by examining the $\mathcal{B}(D^+ \rightarrow \bar{K}^0 e^+ \nu_e)$ using the same $\bar{K}^0(\pi^0 \pi^0)$ selection criteria. We compare the branching fractions measured using alternative $\bar{K}^0(\pi^0 \pi^0)$ mass windows (0.460, 0.505), (0.470, 0.500), (0.480, 0.500) GeV/ c^2 with the nominal value. The maximum change of the re-measured branching fractions 0.9% is taken as the systematic uncertainty. The uncertainty in the $\chi_1^2 + \chi_2^2$ selection method is estimated to be 0.3%, which is the difference of the $\pi^0 \pi^0$ acceptance efficiencies of the hadronic decays of $D^0 \rightarrow K^- \pi^+ \pi^0$ versus $\bar{D}^0 \rightarrow K^+ \pi^- \pi^0$ between data and MC. Adding these in quadrature, we obtain the total independent systematic uncertainty ($\delta_{\text{sys}}^{\text{com}}$) for $\bar{K}^0 \rightarrow \pi^0 \pi^0$ mode to be 2.3%.

Table 2 summarizes the systematic uncertainties in the measurement of $\mathcal{B}(D^+ \rightarrow \bar{K}^0 \mu^+ \nu_\mu)$. Quadratically combining the independent uncertainties for $+-$ and 00 modes after considering their observed DT yields as weights, we obtain the independent uncertainty to be 1.4%. Adding the common and independent uncertainties in quadrature yields the total systematic uncertainty 2.1%.

Table 2 Systematic uncertainties (%) in the measurement of $\mathcal{B}(D^+ \rightarrow \bar{K}^0 \mu^+ \nu_\mu)$. $\delta_{\text{sys}}^{\text{com}}$ and $\delta_{\text{sys}}^{\text{ind}}$ denote the common and independent systematic uncertainties for $+-$ and 00 modes

Common source	Uncertainty	
M_{BC} fit	0.5	
ΔE requirement	0.3	
$M_{\text{BC}} \in (1.863, 1.877)$ GeV/ c^2	0.3	
μ^+ tracking	0.5	
μ^+ PID	0.5	
Topology difference	0.5	
$E_{\max}^{\text{extra } \gamma} < 0.15$ GeV	0.1	
$M_{\bar{K}^0 \mu^+} < 1.6$ GeV/ c^2	0.8	
U_{miss} fit	0.8	
MC generator	0.1	
$\delta_{\text{sys}}^{\text{com}}$	1.6	
Independent source	$\bar{K}^0 \rightarrow \pi^+ \pi^-$	$\bar{K}^0 \rightarrow \pi^0 \pi^0$
π^0 reconstruction	–	2.0
$\bar{K}^0(\pi^+ \pi^-)$ reconstruction	1.5	–
$\bar{K}^0(\pi^0 \pi^0)$ reconstruction	–	0.2
$M_{\pi^0 \pi^0} \in (0.45, 0.51)$ GeV/ c^2	–	0.9
MC statistics	0.4	0.5
Quoted $\mathcal{B}(\bar{K}^0 \rightarrow \pi \pi)$	0.1	0.2
$\chi_1^2 + \chi_2^2$ selection method	–	0.3
$\delta_{\text{sys}}^{\text{ind}}$	1.6	2.3

7 Branching fraction

The branching fraction of $D^+ \rightarrow \bar{K}^0 \mu^+ \nu_\mu$ is determined by

$$\mathcal{B}(D^+ \rightarrow \bar{K}^0 \mu^+ \nu_\mu) = \frac{N_{DT}^{prd}}{N_{ST}^{tot}}, \tag{4}$$

where N_{DT}^{prd} is the DT production yield corrected for detection efficiency and daughter decay branching fractions, which has been constrained to be the same for $+ -$ and 00 modes in the simultaneous fits, and N_{ST}^{tot} is the total ST yield.

Inserting the numbers of N_{DT}^{prd} and N_{ST}^{tot} in Eq. (4), we obtain

$$\mathcal{B}(D^+ \rightarrow \bar{K}^0 \mu^+ \nu_\mu) = (8.72 \pm 0.07 \pm 0.18) \%, \tag{5}$$

where the first uncertainty is statistical and the second systematic.

Furthermore, we examine the measured branching fractions for $D^+ \rightarrow \bar{K}^0 \mu^+ \nu_\mu$ by separately using each of the ST modes, which are shown Fig. 8. We can see that they are consistent with the nominal result within uncertainties very well. Here, the uncertainties are statistical only. The average branching fraction over the six ST modes, weighted by their statistical uncertainties, is $(8.70 \pm 0.07) \%$ and is consistent with our nominal result.

8 Summary and discussion

In summary, by analyzing 2.93 fb^{-1} of data collected at $\sqrt{s} = 3.773 \text{ GeV}$ with the BESIII detector, we measure the absolute branching fraction $\mathcal{B}(D^+ \rightarrow \bar{K}^0 \mu^+ \nu_\mu) = (8.72 \pm 0.07_{stat.} \pm$

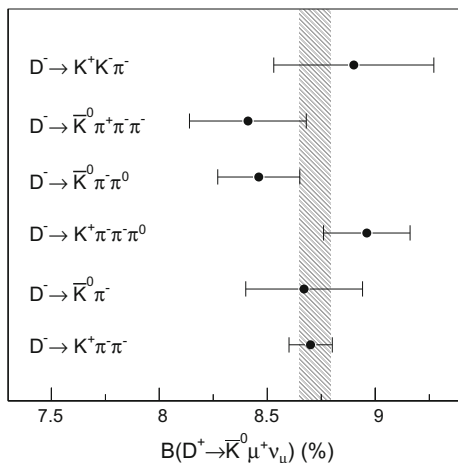


Fig. 8 Comparison of the branching fractions. Dots with error bars are results measured using different ST modes, and shadow band is the nominal result. Only statistical uncertainties are shown

$0.18_{sys.}) \%$, which is consistent with previous measurements within uncertainties but with significantly improved precision. Combining the $\mathcal{B}(D^+ \rightarrow \bar{K}^0 \mu^+ \nu_\mu)$ measured in this work with the $\tau_{D^0}, \tau_{D^+}, \mathcal{B}(D^0 \rightarrow K^- \mu^+ \nu_\mu)$ and $\mathcal{B}(D^+ \rightarrow \bar{K}^0 e^+ \nu_e)$ taken from the world average [2], we determine the ratios of the partial widths $\Gamma(D^0 \rightarrow K^- \mu^+ \nu_\mu) / \Gamma(D^+ \rightarrow \bar{K}^0 \mu^+ \nu_\mu) = 0.963 \pm 0.044$, which supports isospin conservation holding in the exclusive semi-muonic decays of D^+ and D^0 mesons, and $\Gamma(D^+ \rightarrow \bar{K}^0 \mu^+ \nu_\mu) / \Gamma(D^+ \rightarrow \bar{K}^0 e^+ \nu_e) = 0.988 \pm 0.033$, which is consistent with the predicted value in Ref. [1] within uncertainties.

Acknowledgments The BESIII collaboration thanks the staff of BEPCII and the IHEP computing center for their strong support. This work is supported in part by National Key Basic Research Program of China under Contract Nos. 2009CB825204 and 2015CB856700; National Natural Science Foundation of China (NSFC) under Contracts Nos. 10935007, 11125525, 11235011, 11305180, 11322544, 11335008, 11425524; the Chinese Academy of Sciences (CAS) Large-Scale Scientific Facility Program; the CAS Center for Excellence in Particle Physics (CCEPP); the Collaborative Innovation Center for Particles and Interactions (CICPI); Joint Large-Scale Scientific Facility Funds of the NSFC and CAS under Contracts Nos. 11179007, U1232201, U1332201; CAS under Contracts Nos. KJXC2-YW-N29, KJXC2-YW-N45; 100 Talents Program of CAS; National 1000 Talents Program of China; INPAC and Shanghai Key Laboratory for Particle Physics and Cosmology; German Research Foundation DFG under Contract No. Collaborative Research Center CRC-1044; Istituto Nazionale di Fisica Nucleare, Italy; Koninklijke Nederlandse Akademie van Wetenschappen (KNAW) under Contract No. 530-4CDP03; Ministry of Development of Turkey under Contract No. DPT2006K-120470; National Natural Science Foundation of China (NSFC) under Contracts Nos. 11405046, U1332103; Russian Foundation for Basic Research under Contract No. 14-07-91152; The Swedish Resarch Council; U. S. Department of Energy under Contracts Nos. DE-FG02-04ER41291, DE-FG02-05ER41374, DE-SC0012069, DESC0010118; U.S. National Science Foundation; University of Groningen (RuG) and the Helmholtzzentrum fuer Schwerionenforschung GmbH (GSI), Darmstadt; WCU Program of National Research Foundation of Korea under Contract No. R32-2008-000-10155-0.

Open Access This article is distributed under the terms of the Creative Commons Attribution 4.0 International License (<http://creativecommons.org/licenses/by/4.0/>), which permits unrestricted use, distribution, and reproduction in any medium, provided you give appropriate credit to the original author(s) and the source, provide a link to the Creative Commons license, and indicate if changes were made. Funded by SCOAP³.

References

- J.G. Körner, G.A. Schuler, Z. Phys. C **46**, 93 (1990)
- K.A. Olive et al., Particle Data Group, Chin. Phys. C **38**, 090001 (2014)
- Y. Fang, G. Rong, H.L. Ma, J.Y. Zhao, Eur. Phys. J. C **75**, 10 (2015)
- Z. Bai et al., MARKIII Collaboration, Phys. Rev. Lett. **66**, 1011 (1991)
- J.M. Link et al., FOCUS Collaboration, Phys. Lett. B **598**, 33 (2004)
- M. Ablikim et al., BES Collaboration, Phys. Lett. B **644**, 20 (2007)
- M. Ablikim et al., BESIII Collaboration, Chin. Phys. C **37**, 123001 (2013)

8. M. Ablikim et al., BESIII Collaboration, Phys. Lett. B **753**, 629 (2016)
9. M. Ablikim et al., BESIII Collaboration, Nucl. Instrum. Meth. A **614**, 345 (2010)
10. S. Agostinelli et al., GEANT4 Collaboration, Nucl. Instrum. Meth. A **506**, 250 (2003)
11. S. Jadach, B.F.L. Ward, Z. Was, Comput. Phys. Commun. **130**, 260 (2000)
12. S. Jadach, B.F.L. Ward, Z. Was, Phys. Rev. D **63**, 113009 (2001)
13. E.A. Kureav, V.S. Fadin, Sov. J. Nucl. Phys. **41**, 466 (1985)
14. E.A. Kureav, V.S. Fadin, Yad. Fiz. **41**, 733 (1985)
15. E. Barberio, Z. Was, Comput. Phys. Commun. **79**, 291 (1994)
16. D.J. Lange, Nucl. Instrum. Meth. A **462**, 152 (2001)
17. R. G. Ping, Chin. Phys. C **32**, 599 (2008)
18. K. Nakamura et al. (Particle Data Group), J. Phys. G **37**, 075021 (2010). **(and 2011 partial update for the 2012 edition)**
19. J.C. Chen et al., Phys. Rev. D **62**, 034003 (2000)
20. D. Becirevic, A.B. Kaidalov, Phys. Lett. B **478**, 417 (2000)
21. H. Albrecht et al., ARGUS Collaboration, Phys. Lett. B **241**, 278 (1990)
22. M. Ablikim et al., BESIII Collaboration, Phys. Rev. D **92**, 112008 (2015)
23. M. Ablikim et al., BESIII Collaboration, Phys. Rev. D **92**, 072012 (2015)